Analysis of Relationship between Surface Temperature and Shade in an Urban Area by ASTER and PRISM Data

S. Kato [a,*], T. Matsunaga [a], R. Nakamura [b], Y. Yamaguchi [c]

[a] National Institute for Environmental Studies, 16-2 Onogawa, Tsukuba, Ibaraki 305-8506, Japan – (kato.soushi, matsunag)@nies.go.jp
[b] National Institute of Advanced Industrial Science and Technology, 1-1-1 Umezono, Tsukuba, Ibaraki, 305-8568, Japan – r.nakamura@aist.go.jp
[c] Graduate School of Environmental Studies, Nagoya University, D2-1(510), Furo-cho, Chikusa-ku, Nagoya, Aichi 464-8601, Japan – yasushi@nagoya-u.jp

Abstract – According to ASTER TIR data around big cities, surface temperatures on urban centers are often lower than those on the surrounding suburbs. Generally, such patterns are caused by evapotranspiration by vegetation and water, higher heat capacity of buildings, and shadows of buildings. However, 90-m spatial resolution of ASTER TIR limits to analyze contribution of these factors. In order to analyze influence of shade of buildings on surface temperature in urban areas, surface temperature in Tokyo for 20 days during 2000 to 2009 derived from ASTER were compared with shaded fraction estimated from PRISM DEM data. Shaded areas were estimated from DEM and information on solar position recorded with ASTER observation. The deviations of surface temperature were smaller in the places with larger shaded fraction because the land surface was less exposed by solar radiation. This result implies that shadow controls surface temperature equally in spite of the surface types.

Keywords: Surface temperature, Shaded fraction, Urban area, DEM, ASTER, PRISM.

1. INTRODUCTION

In order to analyze thermal environment near land surface including urban areas, remote sensing data has been applied to heat balance analyses in wide areas. The authors have studied estimation of surface heat fluxes by using ASTER and the other satellite data (Kato and Yamaguchi, 2005; Kato and Yamaguchi, 2007; Kato et al., 2008). Though ASTER can observe surface temperature homogeneously in data quality and relatively higher accuracy throughout wide area, it is difficult to obtain detailed spatial pattern of surface temperature in urban area because the spatial resolution is 90 m in Thermal Infrared (TIR) region of ASTER sensor. Because urban surface is constructed by several surface materials including natural and artificial one within small areas, we desire much higher spatial resolution to discern them. However, in the present thermal images from satellite remote sensing, the highest spatial resolution is 90 m of ASTER and 60 m of Landsat ETM+. According to TIR data from satellite sensors, surface temperatures in some urban centers are often lower than those in surrounding areas. Generally speaking, such patterns of surface temperature are caused by higher heat capacity of buildings, evapotranspiration by vegetation and water such as rivers and parks, and shadows of tall buildings. However, abovementioned limitation of spatial resolution prevents to distinguish such influences because urban area is a complex amalgam of the several materials and has quite rough surface. That is, lower and higher temperatures cancel each other in the mixed pixels. Hence, it is important to distinguish subpixel pattern on surface temperature data.

Subpixel analyses of remote sensing data on urban areas has been attempted by choosing soil, water and impervious surface as endmembers in Visible and Near-infrared (VNIR) region and estimate their areal fractions in one pixel as Linear Spectral Mixture Analysis (LSMA) (for example, Ridd, 1995). Rashed et al. (2001) used shadow as an additional endmember for LSMA because of the difference of urban fabric with Ridd (1995). Lu and Weng (2006) selected endmembers of hot- and cold-objects from TIR data as well as impervious surface, soil and vegetation, and compared the relationship between abundances of endmembers and surface temperature using correlation analysis from ASTER data. Although the target site is not urban area, spectral mixture analysis has been also applied for multispectral thermal infrared data, but the purpose of it is to assess material fractions for geological survey using distinctive spectral emissivity of minerals eliminating temperature-related information (Gillespie, 1992). Other than selecting endmembers of typical surface materials in urban areas for LSMA, Tonooka (2005) enhanced ASTER TIR image to 15-m spatial resolution using ASTER VNIR and Shortwave Infrared (SWIR) images based on spectral similarity of the same material.

In VNIR remote sensing, shaded areas are usually treated as useless data because VNIR sensors observe solar irradiance reflected at land surface. On the other hand, since TIR sensors observe thermal radiance emitted from land surface and inevitably atmosphere, TIR images contain information of surface temperature after applying appropriate atmospheric correction even if covered by shadow. In urban areas, shade as well as evapotranspiration limits temperature increase, in contrast with temperature increases on sunlit surface of bare soil and artificial material depending on their heat capacity. According to Meier et al. (2010), for instance, shadows affect long-wave radiation flux for day and night, which means that surface temperature remains lower on the temporally shadowed areas even after shadows disappeared. In this study, the authors were interested in influence of shade on spatial patterns of surface temperature, and tried to detect the relationship between them at the subpixel level. Although the spatial patterns of shade can be extracted by classifying surface types from VNIR images, the authors attempted to estimate them from the information on solar position and the surface geometry obtained from ALOS PRISM Digital Elevation Model (DEM) data which contains the altitudes of

* Corresponding author.

buildings. We analyzed relationships between surface temperature and areal fractions of shade and discussed about the characteristics of surface temperature stay lower by shading in Tokyo, Japan.

2. STUDY AREA AND DATA USED

We choose Tokyo, Japan as our study area because there are many tall buildings and wide roads; hence large shades appear on satellite images. Selected study area is depend on an overwrapped area of ASTER and PRISM images described below and roughly covers central part of Tokyo. Coverage area is about 510 km^2.

We used simultaneous pairs of surface temperature and VNIR level 1B images produced from ASTER data. The spatial resolution of ASTER TIR data is 90 m and is used as basis of this analysis. In order to compare seasonal difference, we used 20 daytime ASTER data taken during 2000 to 2009. Data acquisition dates and their elemental conditions are listed in Table 1. Air temperature was measured on meteorological station in Tokyo (35° 41.3' N, 139° 45.4' E) managed by Japan Meteorological Agency. Solar direction and elevation angles are recorded in metadata of ASTER data products. Figure 1 shows typical spatial distributions of surface temperature from ASTER data for each season. Regardless of seasonal difference, surface temperature is lower in the central part of Tokyo. As the information of surface geometry of the study area, we used DEM data in Tokyo generated from nadir and backward images observed by ALOS PRISM on January 14, 2007 neglecting the landform changes associated with constructions of buildings during the decade. The spatial resolution of PRISM DEM data is 2.5 m. All of ASTER and PRISM DEM data are processed by the National Institute of Advanced Industrial Science and Technology (AIST) GEO Grid.

As a reference map of land use in Tokyo, we used Detailed Digital Information (10 m grid land use map) based on a survey in 1994 published by Geospatial Information Authority of Japan. Although there is a time interval up to 15 years between ASTER data used and the information for land use map, we assume that there are only small changes in land use.

Table 1. Elemental conditions of data acquisition dates

Date	Air temperature (°C)	Solar direction angle (°)	Solar elevation angle (°)
Mar. 29, 00	18.8	154.9	55.1
Nov. 8, 00	21.8	168.8	36.9
Dec. 26, 00	7.2	165.8	29.4
Apr. 1, 01	10.4	152.5	55.7
Jul. 13, 01	34.9	133.3	71.1
Nov. 27, 01	11.0	166.1	31.9
Aug. 10, 02	33.9	136.6	64.2
Oct. 29, 02	16.2	163.9	39.4
Sep. 5, 03	28.7	150.1	58.0
Nov 17, 03	16.3	165.1	34.0
Mar. 8, 04	8.0	151.6	45.6
Apr. 25, 04	16.1	142.6	62.9
Sep. 16, 04	24.1	152.2	53.6
Apr. 28, 05	25.3	141.1	63.7
May 11, 07	21.5	140.0	68.0
Dec. 14, 07	13.2	163.7	29.2
Dec. 30, 07	13.3	161.6	28.6
Jan. 17, 09	8.6	159.0	30.8
Apr. 23, 09	19.4	144.4	62.7
Apr. 30, 09	20.6	143.7	65.4

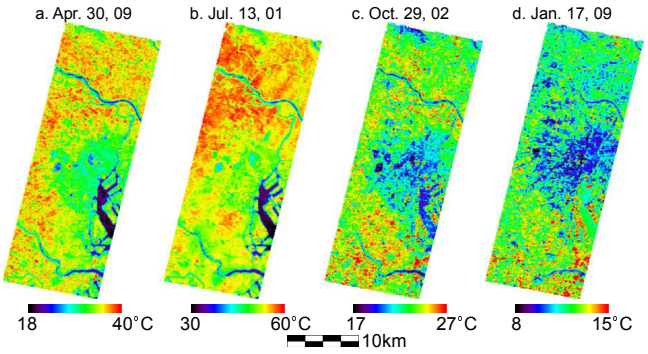

Figure 1. Surface temperature on April 30, 2009 (spring), July 13, 2001 (summer), October 29, 2002 (autumn) and January 17, 2009 (winter) derived from ASTER as typical examples for each season.

3. METHODOLOGY

3.1 Extraction of Shaded Areas from DEM Data

The shaded pixels for each day are extracted from a DEM data by the following procedure. The height difference between the intended pixel and another pixel along the solar direction is estimated. If the solar radiation is interrupted because of larger height difference between the two pixels, the intended pixel is regarded as shaded. Equation (1) and Figure 2 describe the case that the pixel is shaded.

$$dH \geq L \tan \theta \qquad (1)$$

where dH = height difference between the two pixels
L = distance between the two pixels
θ = solar elevation angle

Because DEM data on water body was noisy, we masked the areas coded as "river and lake" and "sea" in Detailed Digital Information assuming change in spatial distribution of water bodies is negligible in spite of temporal and seasonal differences. After that, shaded fractions in 90 m spatial resolution were estimated from spatial distributions of shade in 2.5 m spatial resolution so that shaded areas can be compared with surface temperature from ASTER data.

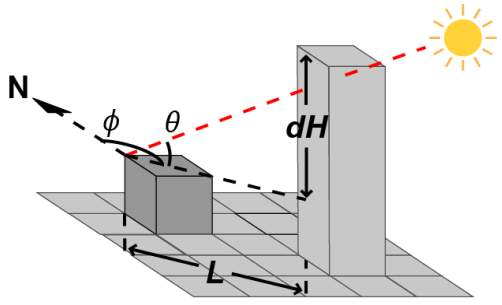

Figure 2. Schematic image of shaded area extraction. θ: solar elevation angle, ϕ: solar direction angle, L: distance between the two pixels, dH: height difference between the two pixels.

3.2 Extraction of Shaded Areas from VNIR Data

For the purpose of checking validity of proposed procedure, the shaded fractions extracted from DEM data were compared with those estimated from shaded areas classified from ASTER VNIR data. Shaded areas were classified by the decision tree method with the spectral thresholds manually selected for each data. However, large water bodies can be misclassified as shaded area because of their similarity of spectral patterns. We corrected such misclassification by masking water body depend on Detailed Digital Information.

4. RESULT AND DISCUSSION

4.1 Spatial Patterns of Shaded Fractions

Typical seasonal patterns of shaded fractions are shown in Figure 3. For all seasons, the shaded fractions are higher in the city centers such as the governmental and commercial districts where some buildings are taller than 200 m. The largest shaded fraction in such areas changed from a few to 100 % mainly according to the solar direction angles. The areas along highways as well as the city centers were shaded more than 30 % and 15 % in winter and autumn, respectively, because of lower solar elevation angles in conjunction with the vertical intervals between highways, roads beneath them and surrounding buildings. Meanwhile small shade along highways almost could not be detected in summer and spring because of higher solar elevation angles.

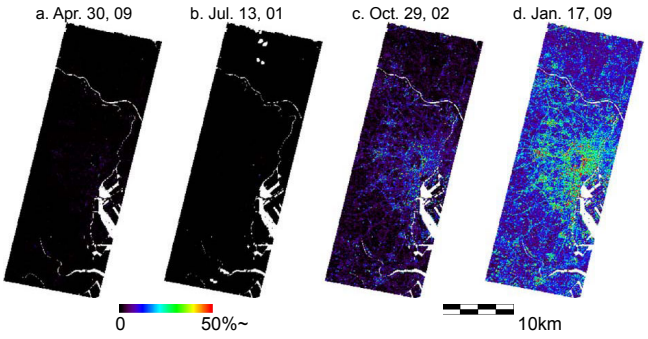

Figure 3. Shaded fractions extracted from PRISM DEM data on April 30, 2009, July 13, 2001, October 29, 2002 and January 17, 2009.

4.2 Comparison between Shaded Fractions from DEM and VNIR Data

Figure 4 shows the typical shaded fractions for each season based on classification of ASTER VNIR data as the examples to compare with Figure 3. The synoptic patterns of shade from DEM and VNIR are quite similar. Both of the shaded area form DEM and VNIR in all of the study area have nonlinear relationships with solar elevation angle as shown in Figure 5. It is consistent with the fact that the length of the shadow is in inverse proportion to tangent of solar elevation angle. However, the shaded fractions in all of the study area estimated from DEM data were six times larger than those from VNIR data in winter because smaller shades could be detected by DEM data and errors were attributed to supervised classification of VNIR data. On the other hand, the shaded fractions were slightly underestimated by DEM data in spring and winter. Because PRISM DEM is generated from stereo pair images, the data cannot depict building shapes accurately even though the spatial resolution is 2.5 m. Therefore, shaded areas are underestimated in the seasons with higher solar elevation angle. Moreover, the shaded fractions by VNIR data can be overestimated when the DN values are smaller than the thresholds but the actual shaded areas are small in the particular pixels because of its 15 m spatial resolution.

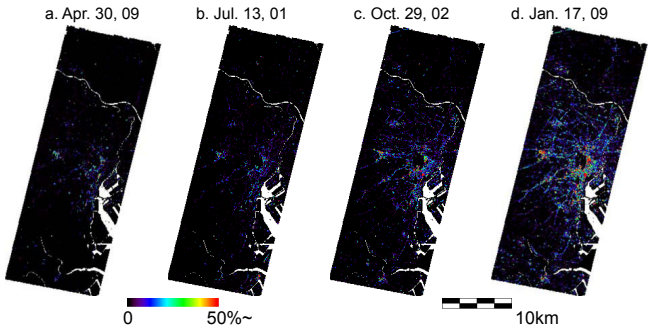

Figure 4. Shaded fractions extracted from ASTER VNIR data on April 30, 2009, July 13, 2001, October 29, 2002 and January 17, 2009.

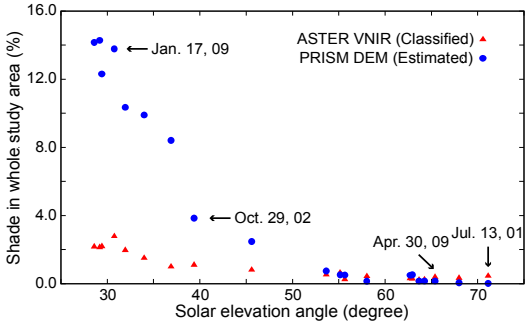

Figure 5. Relation between solar elevation angle and shaded fraction integrated for whole study area estimated from DEM and VNIR data.

4.3 Relationship between Shaded Fraction and Surface Temperature

In winter and autumn, surface temperature was clearly lower than the surroundings on the places largely shaded (see Figures 1, 3 and 4). Seasonal typical patterns of scatter plot between the shaded fraction and surface temperature are shown in Figure 6. There is correlation between neither these two parameters nor surface temperature and land use types. However, the scatter plots show characteristic triangle shapes, namely smaller temperature range in larger shaded fractions in spite of the land use type. Surface temperature slightly tends to affected by surface types in the sunlit areas. Air temperature has no relationship with range of shaded fraction and solar elevation angle because air temperature depends not only on surface heat balance but also on atmospheric condition such as humidity, wind speed and wind direction. These results imply that temperature difference mainly depends on evapotranspiration and thermal properties of sunlit surfaces, in other words, the shadow controls surface temperature equally in spite of the difference of surface coverage.

In winter and autumn, the lowest temperature on shaded areas is close to air temperature despite the value of shaded fraction. On the other hand, the lowest surface temperatures are much higher than air temperatures in autumn and spring. Hence, air temperature cannot be substitution of temperature on shaded surface.

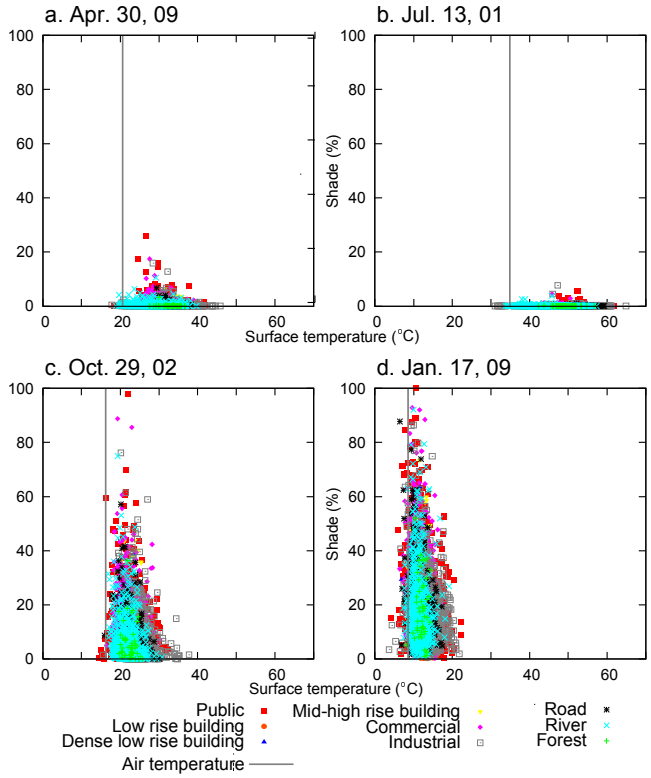

Figure 6. Scatterplots between surface temperature and shaded fraction on April 30, 2009, July 13, 2001, October 29, 2002 and January 17, 2009. Land use type is based on Detailed Digital Information.

5. CONCLUSION

This study estimated areal fraction of shade in Tokyo, Japan from PRISM DEM data and analyzed its effect to surface temperature from ASTER. There is obvious characteristic relationship between shaded fraction and surface temperature. Because larger land surface is shaded in the seasons with lower solar elevation angle, surface temperature data derived from satellite sensor, which is usually observed at nadir, are inevitably affected by shade contamination. Hence, it is necessary to correct for the effect of the shade on surface temperature data before analyzing thermal environment in urban areas in these seasons. This study found that surface temperature on shaded areas are similar in spite of the difference of surface types. Based on the results of this study, surface temperature can be estimated in the shaded places. The authors assume that such information will be applicable to shade correction on surface temperature data.

REFERENCES

A.R. Gillespie, "Spectral mixture analysis of multispectral thermal infrared images," Remote Sens. Environ., vol. 42, p.p. 137-145, November 1992.

S. Kato and Y. Yamaguchi, "Analysis of urban heat-island effect using ASTER and ETM+ data: Separation of anthropogenic heat discharge and natural heat radiation from sensible heat flux," Remote Sens. Environ., vol. 99, p.p. 44-54, November 2005.

S. Kato and Y. Yamaguchi, "Estimation of storage heat flux in an urban area using ASTER data," Remote Sens. Environ., vol. 110, p.p. 1-17, September 2007.

S. Kato, Y. Yamaguchi, C.-C. Liu, and C.-Y. Sun, "Surface heat balance analysis of Tainan City on March 6, 2001 using ASTER and Formosat-2 data," Sensors, vol. 8, p.p. 6026-6044, September 2008.

D. Lu and Q. Weng, "Spatial mixture analysis of ASTER images for examining the relationship between urban thermal features and biophysical descriptors in Indianapolis, Indiana, USA," Remote Sens. Environ., vol. 104, p.p. 157-167, September 2006.

F. Meier, D. Scherer, and J. Richters, "Determination of persistence effects in spatio-temporal patterns of upward long-wave radiation flux density from an urban courtyard by means of Time-Sequential Thermography," Remote Sens. Environ., vol. 114, p.p. 21-34, January 2010.

T. Rashed, J.R. Weeks, and M.S. Gadalla, "Revealing the anatomy of cities through spectral mixture analysis of multispectral satellite imagery: a case study of the Greater Cairo region, Egypt," Geocarto Int., vol. 16, p.p. 5-16, December 2001.

M.K. Ridd, "Exploring a V-I-S (vegetation-impervious surface-soil) model for urban ecosystem analysis through remote sensing: comparative anatomy for cities," Int. J. Remote Sens., vol. 16, p.p. 2165-2185, June 1995.

H. Tonooka, "Resolution enhancement of ASTER shortwave and thermal infrared bands based on spectral similarity," Proc. SPIE, vol. 5657, p.p. 9-19, January 2005.

ACKNOWLEDGEMENTS

This research used ASTER Data beta processed by the AIST GEO Grid from ASTER Data owned by the Ministry of Economy, Trade and Industry, Japan. PRISM DEM data was also generated by the AIST GEO Grid.